TELKOMNIKA, Vol.10, No.8, December 2012, pp. 2285~2294
e-ISSN: 2087-278X
accredited by DGHE (DIKTI), Decree No: 51/Dikti/Kep/2010

PHEVs Park as Virtual Unified Power Flow Controllers

F. R. Islam, H. R. Pota*
School of Engineering and Information Technology (SEIT)
The University of New South Wales at Australian Defence Force Academy (UNSW@ADFA),
Canberra, ACT 2600, Australia
corresponding author, e-mail: F.M.Islam@student.adfa.edu.au, H.R.Pota@adfa.edu.au

Abstract

Unified power flow controllers (UPFCs) are FACTS devices which can fulfil multiple power-flow control objectives, such as the need for reactive shunt compensation, phase shifting and series compensation. However, as they are quite expensive, they are not widely used. In this paper, the potential of a plug-in hybrid electric vehicle (PHEV) in a vehicle-to-grid (V2G) mode of operation using a PHEV charging station to provide a low-cost solution to the design of a virtual UPFC is explained. A third-order dynamic battery model is used to represent the PHEV, and the simulations carried out demonstrate that a PHEV has the potential to work as a virtual UPFC to improve power quality.

Keywords*: PHEVs, Virtual UPFC, Dynamic battery, PHEV's park, V2G Technology*

1. Introduction

The increasing number of PHEV fleets penetrating the market provides an enormous opportunity to use V2G technology to improve the power quality of a utility grid. Statistical data show that more than 95% of personal vehicles remain parked during the day according to a regular schedule [1].A PHEV owner expects his vehicle to be charged during working hours or the time it's parked at home. Ideas for using a PHEV charging station during these periods as a spinning reserve [2], load leveler [3], external storage for renewable energy [4] and filter [5]-[6] have been introduced in various research studies. As reported in [7], a PHEV with a huge capacity battery is able to compensate reactive power to a utility grid while another study has demonstrated that a PHEV battery has the capability to serve as a static compensator (STATCOM) [8]. An effective and economical way of buying and selling electricity from a PHEV according to variable price curves has been reported in [9]-[10]. However, these and other previous studies have not investigated the dynamic behavior of a PHEV battery and its ability to deal with series and shunt compensating strategies as a UPFC does.

In this paper, a comprehensive way of utilizing PHEV batteries and their bidirectional chargers in a charging station as virtual UPFCs in a V2G mode of operation is demonstrated. A smart-park model with the dynamic behavior of a PHEV battery is developed and integrated in a real-life power system. Hybrid-electric power technologies and advances in battery make PHEVs a strong alternative to conventional vehicles and, by the year 2030, their penetration will be 25% [11]. They are the solution to the rising costs of petroleum coupled with increasing financial and energy security requirements and environmental concerns [12], [13]. A PHEV can be charged from both a household's electrical connection and a charging station even when parked during the day. PHEVs give opportunity to design its bidirectional charger as UPFC converters. Any combination of the power system parameters (transmission voltage, line impedance and phase angle) which determine transmittable power can be controlled in real time using a UPFC which can be described as a generalized power flow controller capable of maintaining the certain amounts of real and reactive powers necessary under both normal and temporary system operating conditions. Compared with other FACTs devices, such as STATCOMs and thyristor-controlled series capacitors (TCSCs), it is evident that a UPFC is unique in its capability to control both real and reactive powers [14]. A basic UPFC structure is shown in Figure 1.

Although a UPFC is the most versatile FACTS controller developed so far, it is not widely used for power quality improvement due to its cost which, on average, is twice that of a STATCOM for each KVA [15] while, the most expensive components for the constitution of

Received October 22, 2012; Revised November 24, 2012; Accepted November 28, 2012

FACTS or HVDC devices are their capacitors [16]. In this situation, this paper investigates the possibility of employing a PHEV as a UPFC through its bidirectional converter which has the capability to run in different operational modes according to need, as reported in [17].
The rest of this paper is organized as follows: Section II provides the virtual UPFC model; Section III the controller design; Section IV the test system design and simulation results; and Section VI brief concluding remarks and suggestions for future work.

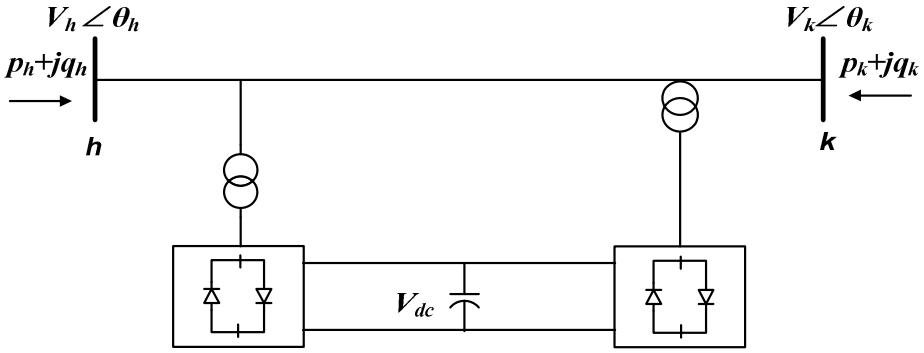

Figure 1. Basic single-line diagram of UPFC

2. Virtual UPFC Model

In order to design a virtual UPFC using a PHEV, it is essential to assess the PHEV's interface with the power system and the dynamics of its battery. As a PHEV needs an electronic converter to connect it to an electrical network for battery charging, a bidirectional converter is considered here as the charger and a dynamic battery model for a PHEV which considers the dynamic responses of electrolytic temperature and the battery's state-of-charge (SOC) is used [5], [6].

The range of PHEV driving required to evaluate battery capacity is considered to be 50 miles/day. As 0.3 kWh of battery energy is required to drive one mile, this means that the capacity of a PHEV battery will be 15 kWh [18], [19].

The controls of the bidirectional converters for the UPFC are designed for $\pm$ 20 MW of power transaction with the grid to represent a park with approximately 1334 vehicles which is a quite reasonable assumption for a typical city. To develop a suitable model of a PHEV, a dynamic model of a rechargeable battery [20], the elements of which are not constant as they depend on both the electrolytic temperature and SOC, is selected. The battery equivalent network is illustrated in Figure 3, where θ represents the electrolytic temperature and I_m is an integral part of the total current (I), as shown in Figure 2.

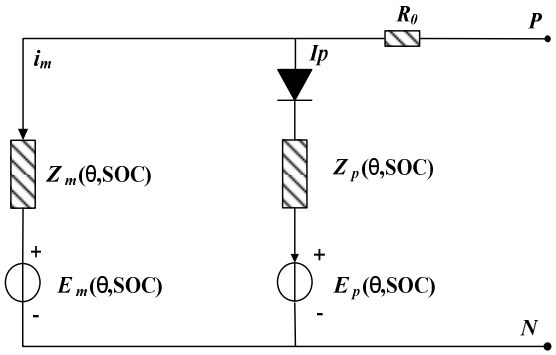

Figure 2. Battery equivalent network with parasitic branch

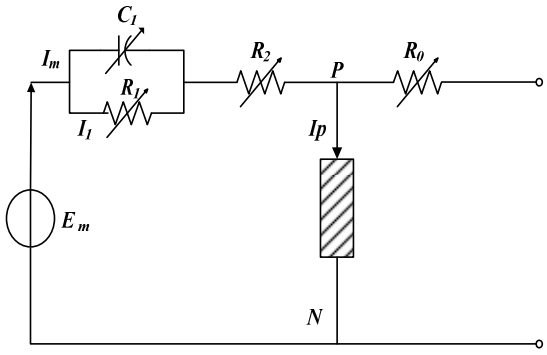

Figure 3. Battery equivalent network

Another part of the total current passes through the parasitic branch. The parasitic reaction is a continuous process that draws current but does not participate in the main reaction. The voltage at this branch is nearly equal to the voltage at the pin and the power dissipated into the real parts of impedances Z_m and Z_p is converted into heat. Impedance of the main reaction branch increases with an increasing charge and, as a result, the terminal voltage of the parasitic branch and the current (I_p) rise. At a battery's full SOC, the impedance of the main reaction branch approaches infinity [20], [21].

This battery model can be represented as an RLC network, as shown in Figure 3, and the number of R-L-C blocks can be limited as the specific speeds of evolution of the electrical quantities evolve very rapidly for PHEVs [20].

The third-order dynamic battery model is designed considering the current, electrolytic temperature and SOC, and its dynamic equations are [20] -[22]:

$$\dot{q}_e = i_{dc}/T_s \quad (1)$$

$$\dot{i}_m = (i_{dc} - i_m)/T_m \quad (2)$$

$$\dot{\theta} = -\frac{1}{C_\theta}[P_s - \frac{\theta - Q_a}{R_\theta}] \quad (3)$$

$$V_{dc} = E_m - V_p(q_e, i_m) + V_e e^{-B_e q_e} - R_0 i_{dc} \quad (4)$$

where V_e represents the hysteresis phenomenon for the lead-acid battery during its charge and discharge cycles. The exponential voltage increases when the battery is charging regardless of its SOC. When the battery is discharging, the exponential voltage decreases immediately while V_p depends on the sign of i_m as:

$$V_p(q_e, i_m) = \begin{cases} \dfrac{R_p i_m + K_p q_e}{SOC} & if i_m > 0 (discharge) \\ \dfrac{R_p i_m}{q_e + 0.1} + \dfrac{K_p q_e}{SOC} & if i_m < 0 (charge) \end{cases}$$

The equations for E_m, R_0, R_1 and R_2 are:

$$E_m = E_{m0} - K_e(273 + \theta)(1 - SOC) \quad (5)$$

$$R_0 = R_{00}[1 + A_0(1 - SOC)] \quad (6)$$

$$R_1 = -R_{10} ln(DOC) \quad (7)$$

$$R_2 = R_{20} \frac{exp[A_{21}(1 - SOC)]}{1 + exp(A_{22} I_m / I^*)} \quad (8)$$

where E_{m0}, K_e, R_{00}, A_0, A_{21} and A_{22} are constant for a particular battery.

The SOC and depth of charge (DOC) can be expressed as:

$$SOC = \frac{Q_n - Q_e}{Q_n} = 1 - q_e \quad (9)$$

$$DOC = 1 - Q_e / C(I_{avg}, \Theta) \quad (10)$$

where C_θ and *Ps* are the battery's thermal capacity and power, respectively, R_0 the thermal resistance, Q_a the ambient temperature, Q_e the extracted capacity in Ah, and Q_n the rated

battery capacity in Ah. K_c, E_m, E_{m0}, K_e, R_{00}, A_0, A_{21} and A_{22} are constant for a particular battery the parameters are available in [20].

As the parasitic branch's behavior is strongly nonlinear, its current can be expressed as:

$$I_p = V_p G_p \exp(\frac{V_p}{V_{po}} + Ap(1 - \frac{\theta}{\theta_f})) \quad (11)$$

The computation of R_p gives the heat produced by the parasitic reaction by means of the Joule law: $P_s = R_p I_p^2$

Therefore, our proposed UPFC model can be represented by Figure 4. Research has been carried out [8] to examine the P-Q capability of a PHEV battery and, as shown in Figure 5 that of a real battery [23] varies within $\pm$ 138 kW and $\pm$ 138 kVA respectively.

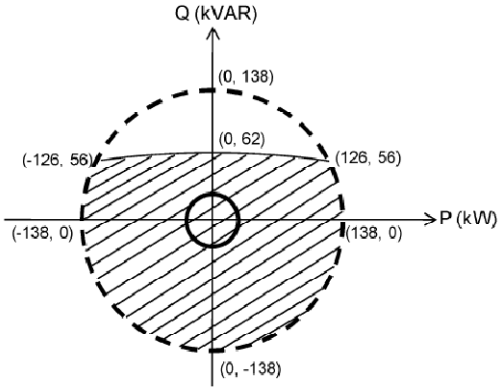

Figure 5. PQ capability of a Vehicle battery [8]

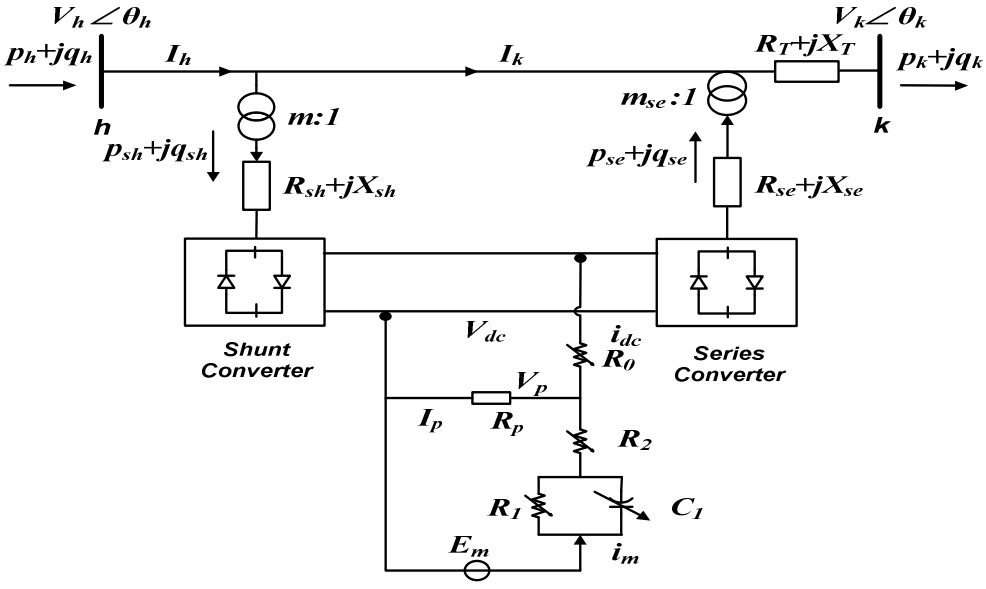

Figure 4. Virtual UPFC model using PHEV

3. Controller Design

As the UPFC is realized as a combination of series and shunt converter-based FACTS devices with a common DC voltage (V_{dc}), we have two different strategies for controlling its converters using simple controller structures; the shunt converter by controlling

the AC and DC voltages to obtain the firing angle (α) and modulating amplitude (m) and the series converter by a simple decoupling controller for the active and reactive powers.

3.1 Shunt Converter Control

A bidirectional converter (a rectifier and an inverter) and a transformer with reactance x_{sh}, as depicted in Figure 6, are used. The DC voltage is regulated by means of the converter's m as [22]:

$$m = \frac{x_{sh}}{V_s k V_{dc}} \sqrt{p_s^2 + \left(q_s + \frac{V_s^2}{x_{sh}} \right)^2} \tag{12}$$

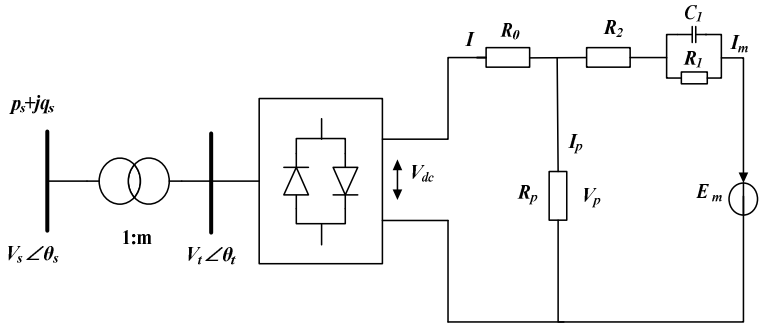

Figure 6: Shunt converter connection with PHEV in network

As the DC power of the battery ($P_{dc} = V_{dc} I$) is considered to be the real power in the network ($p_s = P_{dc}$), its link with the AC network is:

$$p_s = \frac{V_t V_s}{x_{sh}} \sin(\theta_t - \theta_s) = V_{dc} I \tag{13}$$

$$q_s = \frac{V_t V_s}{x_{sh}} \cos(\theta_t - \theta_s) - \frac{V_s^2}{x_{sh}} \tag{14}$$

where $V_t = kmV_{dc}$ and the rectifier gain $k = \sqrt{(3/8)}$. Therefore, the relationship between θ_t and θ_s can be expressed as:

$$\theta_t = \theta_s + a\sin\left(\frac{x_{sh} I}{kmV_s}\right) \tag{15}$$

and the final equation for q_s is:

$$q_s = \frac{V_s^2}{x_{sh}} - \frac{V_s kmV_{dc}}{x_{sh}} \sqrt{1 - \left(\frac{x_{sh} I}{kmV_s}\right)^2} \tag{16}$$

where p_s is the real power, q_s the reactive power, V_s the voltage, θ_s the phase angle at the connecting bus, and V_t and θ_t the voltage and phase angle before the transformer, respectively. The PHEV is connected to the AC network through the bidirectional converter which is completed by the control that regulates m and α. Special care is taken to develop the operating limits of the converter, with both α and m limited by the boundary conditions as:

$$\alpha^{min} \le \alpha \le \alpha^{max}$$
$$m^{min} \le m \le m^{max}$$

The PHEV's battery current (i_m) is subjected to a constant power control as:

$$\dot{i}_m = \frac{1}{T_m}[\frac{V_{dc} i_{dc}^{lim}}{E_{m0}} - i_m] \quad (17)$$

The battery current set point is limited by the SOC and then the currents i_{shd} and i_{shq} are regulated through a set of PI controllers, as shown in Figure 7. V_{shdr} and V_{shqr} determine the m and α, respectively, passing through another set of PI controllers which can be expressed by the following equations:

$$\dot{m} = (K_m(V_{ref} - V_s) - m)/T \quad (18)$$
$$\dot{x}_a = K_i(V_{ref} - V_s) \quad (19)$$
$$0 = K_p(V_{ref} - V_s) + x_a - \alpha \quad (20)$$

where $V_s = \sqrt{V_{shd}^2 + V_{shq}^2}$

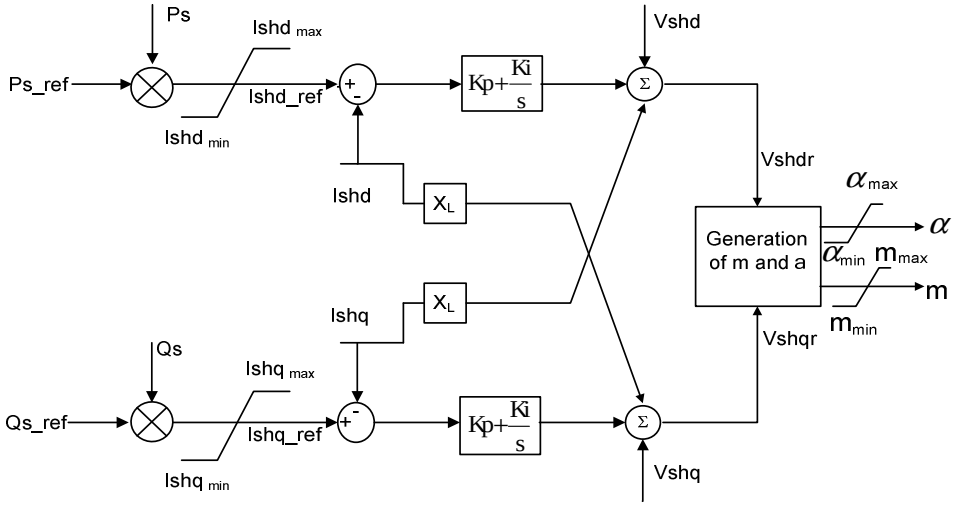

Figure 7. Modified decoupled P-Q controller for shunt converter [7]

3.2 Series Converter Control

The decoupled P-Q controller shown in Figure 8 is used to control the series converter of the virtual UPFC. The output variables X_1 and X_2 of the PI controller are used to calculate the series converter's output voltages V_{sed} and V_{seq}, respectively. The dynamic equations for the series converter can be expressed as [22]:

$$\dot{x}_1 = K_I(\frac{2Pk_{ref}}{V_{kd}} - I_{kd}) \quad (21)$$
$$\dot{I}_{kd} = x_1 - KI_{kd} + K_p(\frac{2P_{kref}}{V_{kd}} - I_{kd}) \quad (22)$$

$$\dot{x}_2 = K_I(\frac{2Qk_{ref}}{V_{kd}} - I_{kq}) \tag{23}$$

$$\dot{I}_{kq} = x_2 - KI_{kq} + K_p(\frac{2Q_{kref}}{V_{kd}} - I_{kd}) \tag{24}$$

Other control parameters are:

$$K = \frac{R_T + R_{se}}{X_T + X_{se}}\Omega \tag{25}$$

$$V_{kd} = \sqrt{2}Vk \tag{26}$$

$$V_{hd} = \sqrt{2}Vh\cos(\theta_k - \theta_h) \tag{27}$$

$$V_{hq} = \sqrt{2}Vh\sin(\theta_k - \theta_h) \tag{28}$$

$$x_1 = x_1^* + K_I(\frac{2Pk_{ref}}{V_{kd}} - \Omega I_{kd}) \tag{29}$$

$$x_2 = x_2^* + K_I(\frac{2Qk_{ref}}{V_{kd}} + \Omega I_{kd}) \tag{30}$$

$$V_{sed} = V_{hd} - V_{kd} - \frac{X_T - X_{se}}{\Omega}X_2 \tag{31}$$

$$V_{seq} = V_{hd} - \frac{X_T - X_{se}}{\Omega}X_2 \tag{32}$$

$$V_{se} = \frac{1}{\sqrt{2}}\sqrt{V_{sed}^2 + V_{seq}^2} \tag{33}$$

$$m_{se} = \sqrt{\frac{8}{3}}(\frac{V_{se}}{V_{dc}}) \tag{34}$$

where Ω is the fundamental frequency base in rad/s.

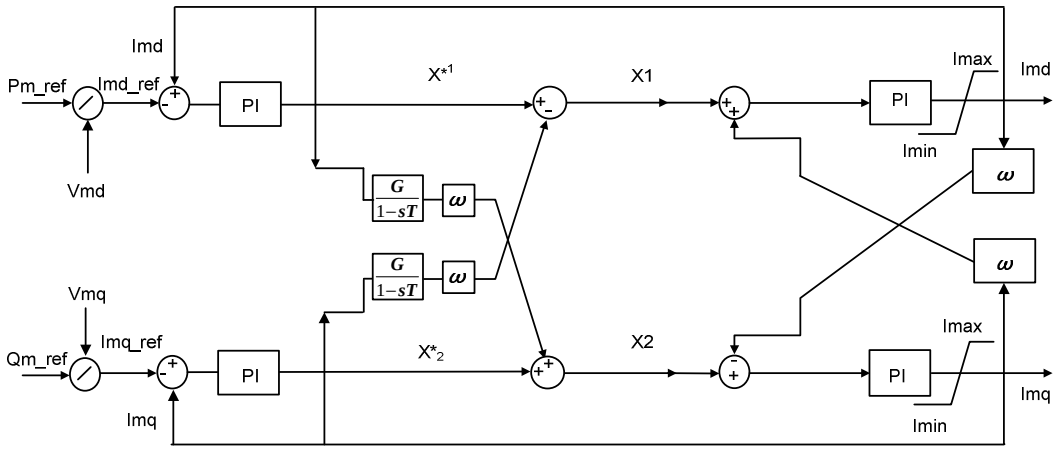

Figure 8. Decoupled P-Q controller for series converter [24]

The DC voltage is controlled within its maximum and minimum limits by a set of PI controllers, as shown in Figure 9.

4 Test System Design

To validate the proposed UPFC model, the test system shown in Figure 10, which operates at 230 kV with two Thevinen impedance sources connected via transmission lines, and a T-tap terminated with a Δ-Y transformer and rated at 230 kV/25 kV, is introduced. The Y-Y connected shunt transformer of the UPFC is rated at 20 MVA and 230kV/21kV, and the Y-Δ connected series transformer at 20 MVA and 92kV/21kV.

Figure 9. DC voltage controller

Figure 10. 6-bus test system for virtual UPFC

5 Simulation Results

In commendations to PHEV's Parks as virtual UPFC, two types of simulation results are presented. In the first phase of study, internal output and the reference value of currents are presented to know the characteristics of virtual UPFC. In the second phase of study, the achievement of the virtual UPFC is compared with a standard UPFC when it is connected amid bus 3 and bus 2 and a fault has been applied amid bus 4 and bus 5 at t=0.5 sec and abolish at t=0.75 Sec. Figure 11 and Figure12 show the q axis current for shunt and series converter respectively and Figure 13 and Figure 14 are the current of q axis for shunt and series converte respectively. All the current show that the output d and q axis current of shunt and series converter follow the reference current before and after fault.

A comparison study has been made between a standerd and the virtual UPFC to varify the performance of the proposed UPFC in the network shown in Figure 10. In Figure 15, red color shows the standard and green color shows the VUPFC's voltage output during the fault and normal condition where the performance of VUPFC is quite satisfactory with comparison of a standard UPFC.

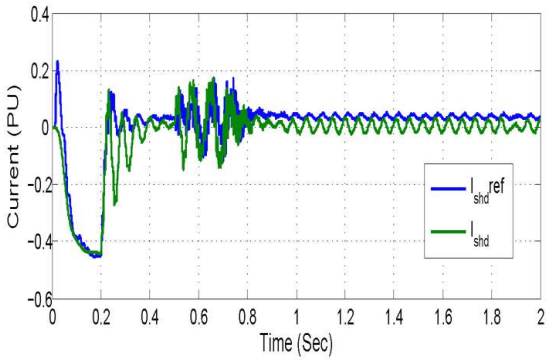

Figure 11. Shunt converter d axis current of Virtual UPFC

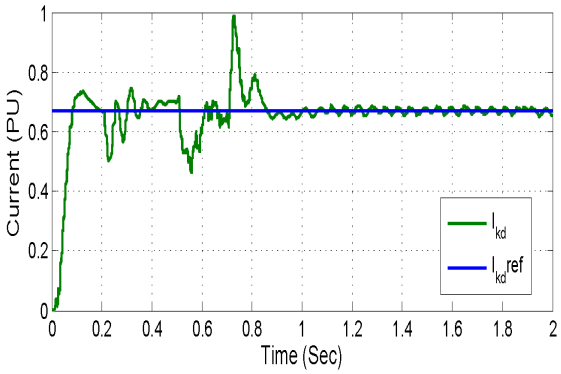

Figure 12. Series converter d axis current of Virtual UPFC

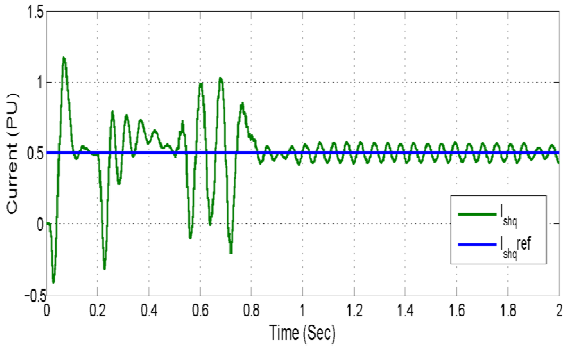

Figure 13. Shunt converter q axis current of Virtual UPFC

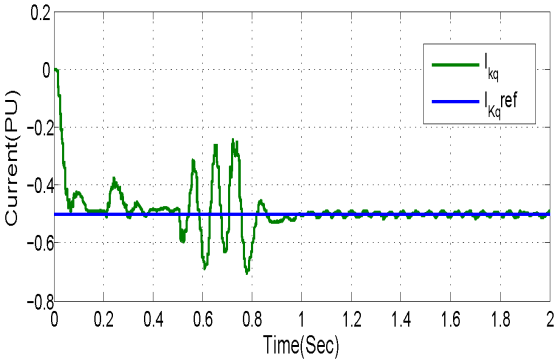

Figure 14. Shunt converter q axis current of Virtual UPFC

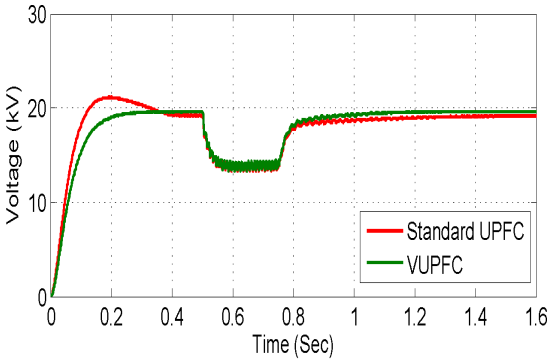

Figure 15. Output voltage from UPFCs

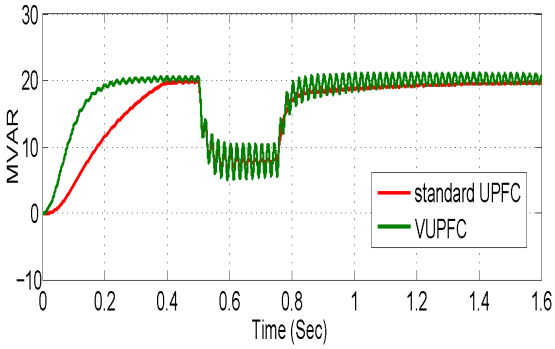

Figure 16. Reactive power support from UPFCs

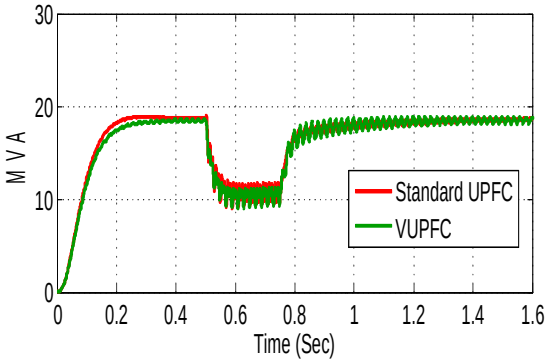

Figure 17. Real power support from UPFCs

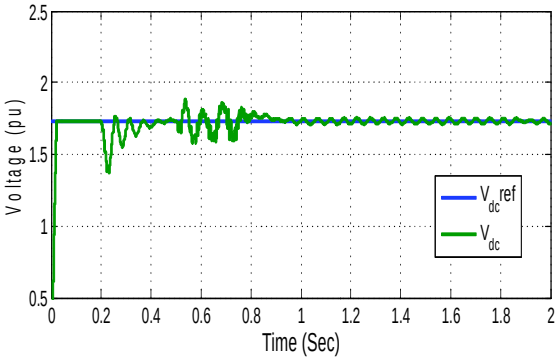

Figure 18. Output DC voltage from VUPFC

The reactive and real power support shown in Figure 16 and Figure 17, from the VUPFC for the netwok are in the same level with comparison to standard UPFC but the oscilation in the out of VUPFC is much higher for both of the cases. In this work we have used very simple converter controllers, however by designing proper controllers this problem can be minimized. At Figure 18 the DC voltage from the PHEVs park is shown which assure the reference level.

6 Conclusion

The goal achieved via this study was an investigation into the performance of a dynamic PHEV as a virtual UPFC in terms of both the voltages of its series and shunt converters and the system's current. To assess the accuracy of the designed system, we compared the output of

the virtual UPFC with a UPFC rated at the same standard. The results obtained from simulations showed that the PHEV had the capability to work as a virtual UPFC to improve power quality. However, a great deal of research is needed to study the implementation of V2G technology in a power system. Several issues, such as the consequences of battery ageing and achieving improvements in the control technique considering smart-grid technology to obtain better performances from the virtual UPFC could be interesting topics for future work.

Acknowledgements

This work has been supported by The University of New South Wales @ The Australian Defence Force Academy, Canberra, Australia

References

[1] J. Tomi´c, W. Kempton, Using fleets of electric-drive vehicles for grid support, *Journal of Power Sources* 2007; 168 (2): 459-468.
[2] W. Kempton, J. Tomi´c, Vehicle-to-grid power fundamentals: Calculating capacity and net revenue, *Journal of Power Sources* 2005; 144 (1): 268-279.
[3] C. Guille, G. Gross, A conceptual framework for the vehicle-to-grid V2G implementation, *Energy Policy* 2009; 37 (11): 4379-4390.
[4] W. Kempton, J. Tomi´c, Vehicle-to-grid power implementation: From stabilizing the grid to supporting large-scale renewable energy, *Journal of Power Sources* 2005; 144 (1): 280-294
[5] F. R. Islam, H. R. Pota, *Design a PV-AF system using V2G technology to improve power quality*, Proceedings of the 37th Annual Conference on IEEE Industrial Electronics Society, IECON 2011; 861-866.
[6] F. R. Islam, H. R. Pota, M. S. Ali, *V2G technology for designing active filter system to improve wind power quality*, Proceedings of the 21st Australasian Universities Power Engineering Conference (AUPEC), 2011; 1–6.
[7] F. R. Islam, H. R. Pota, *V2G technology to improve wind power quality and stability, in: Australian Control Conference (AUCC)*, 2011; 452-457.
[8] P. Mitra, G. Venayagamoorthy, K. Corzine, Smartpark as a virtual statcom, *IEEE Transactions on Smart Grid*, 2011; 2 (3): 445-455.
[9] C. Hutson, G. Venayagamoorthy, K. Corzine, *Intelligent scheduling of hybrid and electric vehicle storage capacity in a parking lot for profit maximization in grid power transactions*, Proceedings of the Energy 2030 Conference, 2008; 1-8.
[10] A. Y. Saber, G. K. Venayagamoorthy, Intelligent unit commitment with vehicle-to-grid a cost-emission optimization, *Journal of Power Sources* 2010; 195 (3): 898-911.
[11] S. W. Hadley, A. A. Tsvetkova, Potential impacts of plug-in hybrid electric vehicles on regional power generation, *The Electricity Journal* 2009; 22 (10): 56–68.
[12] D. M. Lemoine, D. M. Kammen, A. E. Farrell, An innovation and policy agenda for commercially competitive plug-in hybrid electric vehicles, *Environmental Research Letters* 2008; 3 (1): 014003.
[13] M. P. C. Agency, *Air emissions impacts of plug-in hybrid vehicles in Minnesota's passenger fleet*, Minnesota Pollution Control Agency. Report number:032907013010. 2007.
[14] Y. H. Song, A. T. Johns (Eds.), Flexible ac transmission system (FACTS), The Institution of Electrical Engineers, London, 1999
[15] R. Mathur, R. Varma, Thyristor-Based FACTS Controllers for Electrical Transmission Systems, IEEE Press Series on Power Engineering, 2002
[16] E. W. Kimbark, Direct Current Transmission, Wiley-Interscience. 1971
[17] M. Kisacikoglu, B. Ozpineci, L. Tolbert, *Examination of a phev bidirectional charger system for V2G reactive power compensation*, Proceedings of the Twenty-Fifth Annual IEEE Applied Power Electronics Conference and Exposition (APEC), 2010; 458-465
[18] A. Ipakchi, F. Albuyeh, Grid of the future, *IEEE Power and Energy Magazine,* 2009; 7 (2): 52-62.
[19] K. Clement-Nyns, E. Haesen, J. Driesen, The impact of charging plug-in hybrid electric vehicles on a residential distribution grid, *IEEE Transactions on Power Systems*, 2010; 25 (1): 371-380
[20] M. Ceraolo, New dynamical models of lead-acid batteries, *IEEE Transactions on Power Systems,* 2000; 15 (4): 1184-1190.
[21] S. Barsali, M. Ceraolo, Dynamical models of lead-acid batteries: implementation issues, *IEEE Transactions on Energy Conversion,* 2002; 17 (1): 16-23
[22] F. Milano, "Power System Modelling and Scripting" New York: Springer-Verlag, 2010
[23] Saft hybride electric military vehicle data sheet. URL http://www.saftbatteries.com/
[24] E. Uzunovic, C. Canizares, J. Reeve, *Fundamental frequency model of unified power flow controller*, Proceedings of the North Amirican Power Symposium (NAPS), 1998; 294–299